

Laser pulses for coherent xuv Raman excitation

Loren Greenman,^{1,2} Christiane P. Koch,³ and K. Birgitta Whaley^{1,2,*}

¹*Department of Chemistry and Kenneth S. Pitzer Center for Theoretical Chemistry, University of California, Berkeley, CA 94720, USA*

²*Chemical Sciences, Lawrence Berkeley National Laboratory, Berkeley, CA 94720, USA*

³*Theoretische Physik, Universität Kassel, Heinrich-Plett-Str. 40, D-34132 Kassel, Germany*

(Dated: November 21, 2021)

We combine multi-channel electronic structure theory with quantum optimal control to derive Raman pulse sequences that coherently populate a valence excited state. For a neon atom, Raman target populations of up to 13% are obtained. Superpositions of the ground and valence Raman states with a controllable relative phase are found to be reachable with up to 4.5% population and phase control facilitated by the pump pulse carrier envelope phase. Our results open a route to creating core-hole excitations in molecules and aggregates that locally address specific atoms and represent the first step towards realization of multidimensional spectroscopy in the xuv and x-ray regimes.

Multidimensional spectroscopy in the infrared [1] and uv-vis [2, 3] spectral regions has proven to be a powerful tool for revealing quantum coherent dynamics in biological systems [4] and quantum devices [5–7]. Extending the techniques of multidimensional spectroscopy to the xuv and x-ray regimes could open the door to studying energy transfer between different atomic sites in molecules [8, 9]. It would provide a local probe of valence excitations, which would be invaluable for studies of energy transfer processes in biological systems and quantum devices. However, this presents novel challenges, since the large energy of the xuv and x-ray pulses can result in a high probability of ionization, while selective excitation of a specific intermediate state may be hampered by the presence of a multitude of other states closely lying by.

On an abstract level, these difficulties reflect the problem of controllability when a continuum of states is involved [10]. Controllability addresses the question whether a quantum control target is reachable, given the properties of the Hamiltonian [11]. For a structureless continuum, no control is expected, whereas resonances in the continuum are predicted to facilitate control [12], the extent of which depends on the resonance lifetime compared to the duration of the pulses. Standard controllability analysis [11] cannot account for finite lifetimes and is thus not applicable. This leaves numerical optimization as the method of choice to investigate how much control is attainable for a process that necessarily proceeds via a continuum of states.

Here we combine quantum optimal control theory with the time-dependent configuration interaction singles (TDCIS) description of electronic structure to assess the feasibility of coherent xuv Raman excitation, as a first step towards multidimensional spectroscopy in the x-ray regime [8]. Achieving such coherent Raman excitation with a high yield is extremely challenging, due to the presence of the ionization continuum that is accessible by both pump and Stokes pulses. Furthermore, in order to probe electronic dynamics of valence excitations

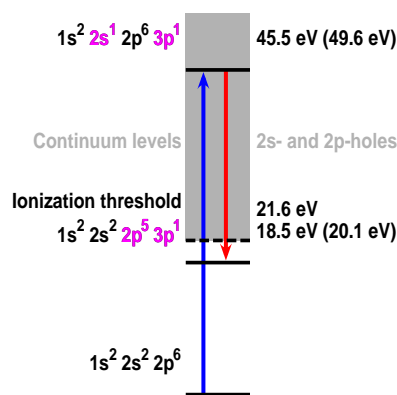


FIG. 1. (Color online) Targeted coherent xuv Raman process in neon. The experimental energies are shown together with TDCIS values in parentheses.

in molecules, the capability to prepare coherent superpositions of valence states is imperative, in addition to population transfer into the excited states. The primary control objectives are thus to both drive population to a specific atomic valence excitation and to achieve a coherent superposition of ground state and valence excitation with controllable relative phase. We demonstrate here that optimal control theory allows us to predict experimentally feasible pulse forms that populate the desired state up to 13% and achieve superpositions of ground and excited state with arbitrary relative phase and up to 4.5% excited state population. The optimal control approach not only allows for generating the pulse forms but also reveals insight into the physical mechanism of the optimized excitation process. This, in turn, allows development of simpler pulse sequences with similar performance but better compatibility with experimental constraints. Our work is the first to tackle the problem of the presence of the electronic continuum by optimal control, adding an important capability to the growing attempts now underway to tailor multi-electron dynamics [13–16].

We consider as example the neon atom, employing the levels shown in Fig. 1. They are accessible in table-top experiments generating intense high harmonics [17] or using a free-electron laser operating in the xuv regime. A pump pulse of 45.5 eV couples the ground state, with configuration $1s^2 2s^2 2p^6$, to the core-excited resonance ($1s^2 2s^1 2p^6 3p^1$), driving a $2s-3p$ hole-particle excitation. A Stokes pulse of 27.0 eV induces the filling of the $2s$ hole with a $2p$ valence electron, creating the $2p-3p$ excitation ($1s^2 2s^2 2p^5 3p^1$) which is the target valence excited state.

In order to describe the manifold of excited states and capture the ionizing electron density, we calculate the quantum dynamics using the time-dependent configuration interaction singles (TDCIS) method on a numerical grid with a complex absorbing potential (CAP) [18, 19]. The TDCIS method was developed to capture channel coupling in high harmonic generation [18, 20], and it has been used to describe multichannel dynamics in a number of ultrafast processes [21–24]. The wavepacket is described by a single-determinant Hartree-Fock ground state $|\Phi_0\rangle$, single-particle excitations from occupied orbital i to unoccupied orbital a $|\Phi_i^a\rangle$, and time-dependent coefficients α ,

$$|\Psi(t)\rangle = \alpha_0(t)|\Phi_0\rangle + \sum_{i,a} \alpha_i^a(t)|\Phi_i^a\rangle. \quad (1)$$

The dynamical equations for the coefficients are obtained by inserting Eq. (1) into the Schrödinger equation [18]. A complex absorbing potential (CAP) is added to the Hamiltonian in order to capture ionization [18, 25, 26].

We may simplify the electronic structure calculation by employing a Hartree-Fock-Slater one-electron potential as a starting point (TDCIS-HFS). Dynamical calculations with TDCIS-HFS are found to yield final state populations agreeing with full TDCIS results to within a factor of three. A further gain in efficiency is possible by using a simplified configuration space including only ionization levels reachable by one-photon absorption within a bandwidth of a few eV (TDCIS-HFS-1P). Pulse sequence optimizations were performed using the TDCIS-HFS-1P method, and propagations were performed with the optimal pulses at the full TDCIS level. All calculations employed 1000 grid points in 63.6 \AA , with a CAP radius of 42.4 \AA and CAP strength of 10^{-4} , with angular momentum functions restricted to $L \leq 3$.

Krotov’s optimal control method [27–30] is utilized to find pulses which suppress ionization. It minimizes the cost function J for the desired excitation,

$$J_{t_f} = -|\langle \Phi_D | \Psi(t_f) \rangle|^2, \quad (2)$$

where $|\Phi_D\rangle$ represents the target state (the $2p$ - $3p$ excitation) and $\Psi(t_f)$ the time evolved state in presence of the external field $\mathcal{E}(t)$. The Krotov pulse update formula is given by [30]

$$\mathcal{E}(t)^{(k+1)} = \mathcal{E}(t)^{(k)} - \frac{\lambda}{2S(t)} \text{Im} \left(\chi(t)^T \mathbf{z} \alpha(t)^{(k+1)} \right), \quad (3)$$

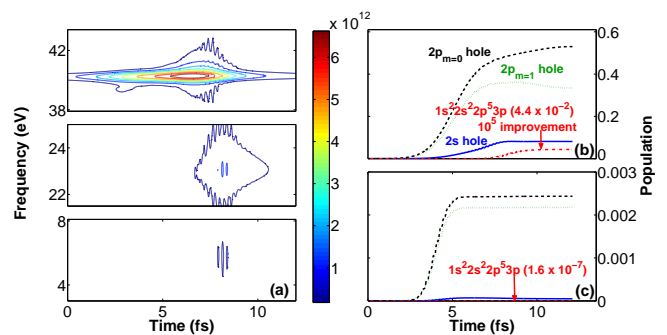


FIG. 2. (Color online) (a) Filtered Wigner distribution of the optimized pulse sequence, showing the Stokes pulse starting at the end of the pump pulse and addition of low frequency components. Color bar units are W/cm^2 . (b) Populations of $2p$, $2s$ hole states and the target $1s^2 2s^2 2p^5 3p$ state that are achieved with the optimized pulse. (c) Populations for two simultaneous 2.0 fs TL pulses with central frequencies of 49.6 eV and 29.5 eV . The population of the target state (dashed-dotted red line) reaches 4.4×10^{-2} for the optimized pulse, compared to $\sim 1.6 \times 10^{-7}$ for the naive sequence. The $2p$ holes ($m = 0$; black dashed line, $m = 1$; green dotted line) correspond to $1s^2 2s^2 2p^5 nl$ configurations, the $2s$ hole (blue solid line) to $1s^2 2s^1 2p^6 nl$ configurations.

where $\mathcal{E}_t^{(k)}$ is the time-dependent field amplitude at the k -th iteration, $S(t)$ an arbitrary shape function which ensures that the pulse goes to zero at the ends of the time propagation, \mathbf{z} the transition dipole matrix in the basis of TDCIS states, α a vector of the time-dependent coefficients of Eq. (1), and χ the set of corresponding time-dependent co-vectors [27]. The choice of cost function at the final time determines the “initial condition” [27],

$$\chi(t_f) = 2\alpha_D (\alpha_D^T \alpha(t_f))^*. \quad (4)$$

The covectors $\chi(t)$ are propagated backwards in time according to the equations of motion,

$$\dot{\chi} = i \left(\mathbf{H}^T - \mathcal{E}(t)^{(k)} \mathbf{z}^T \right) \chi(t), \quad (5)$$

with \mathbf{H} the time-independent part of the Hamiltonian [31].

Our starting point is a naive pulse sequence for the Raman process obtained by assuming simultaneous, transform-limited (TL) pump (p) and Stokes (S) pulses, $\mathcal{E}_{p/S}(t) = \mathcal{E}_{0,p/S} \sin(\omega_{p/S}(t - t_{0,p/S}) + \phi_{p/S}) \exp[-4 \ln 2 (t - t_{0,p/S})^2 / \sigma_{p/S}^2]$, with parameters corresponding to the experimental setup of Ref. [17]: a full-width at half maximum (FWHM) duration of 2 fs and a peak intensity of $3.5 \times 10^{12} \text{ W}/\text{cm}^2$. This sequence does not populate the Raman state significantly, cf. Fig. 2(c). The overall depopulation of the ground state is small, of order 10^{-3} . This population is divided between $2p$ holes and the $2s$ hole. The target state is one particular configuration of the $2p$ hole which is populated only to a few hundredths of a percent of the total hole population.

Starting with the naive pulse sequence, an optimized sequence is obtained using Krotov's method. The resulting pulses, shown in Fig. 2(a), achieve the Raman excitation with a population of 4.4×10^{-2} , five orders of magnitude better than the starting pulse. The optimized pulse is increased in amplitude by a factor of about 16 and therefore ionizes more of the electron density. It nevertheless yields an improvement of three orders of magnitude in the percentage contribution of the target state to the total hole probability. The peak intensity of the optimal sequence is about 7.9×10^{14} W/cm². Analysis of the dynamics under the optimized pulse reveals the added low frequency contribution (Fig. 2(a)) to be irrelevant, whereas the relative timing of the pump and Stokes pulse components are key features. In particular, the relative timing of the Stokes pulse, which now enters only at the end of the pump pulse, is critical. As developed further below, this suggests a sequential mechanism that may be used to further optimize the pulse sequence within experimental constraints.

Coherent superpositions of the Raman state with the ground state are obtained by optimizing with $0.99e^{i\phi_t}|1s^22s^22p^53p\rangle + 0.16|1s^22s^22p^6\rangle$ as target state in the cost function (2), where ϕ_t is the desired relative phase. This target state was empirically determined to drive population to the Raman excited state while maintaining the target phase with the ground state. In this type of optimization, both amplitude and phase of the pulse sequence are varied. This procedure enables identification of pulses for arbitrary, prespecified values of the target phase ϕ_t . Figure 3(a) shows the phase error in the target state as a function of ϕ_t . The optimized pulses have a combined peak intensity of about 10^{14} W/cm² and excite a Raman population of 4.5% while depopulating the ground state by about 53%. Independent of the value of ϕ_t , all optimizations are found to converge on the same pulse envelopes that strongly resemble a time-separated pump and Stokes pair, with the Stokes pulse starting just after the peak of the pump pulse, cf. Fig. 3(c). The optimized pulses differ primarily in the value of the carrier envelope phase (CEP) of the pump component, ϕ_p , calculated using a Hilbert transform of the pulse [32]. It is found to correlate closely with the target phase ϕ_t , cf. Fig. 3(b). Since the propagation of the excited state after the pulse imparts a phase on the excited state that depends on an arbitrary origin of time t_{origin} , $e^{-i\omega(t-t_{origin})}$, we picked t_{origin} so that a phase of 0.0 was obtained by the pulse with a CEP of 0.0. The correlation between target phase and pump CEP is rationalized by the pump imprinting its CEP onto the intermediate state, which yields the desired relative phase between intermediate and Raman state. These results show that a coherent superposition can be excited with any desired relative phase ϕ_t merely by changing the pump pulse CEP ϕ_p , once the optimized pulse envelope has been determined.

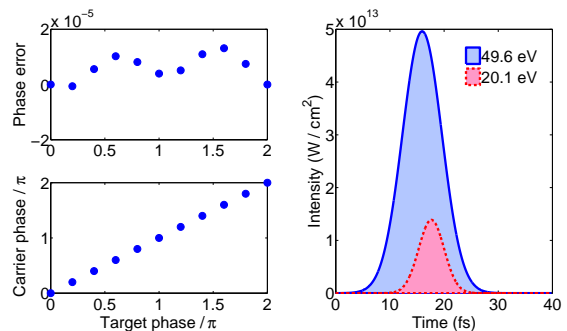


FIG. 3. (Color online) Optimization of coherent superpositions: (a) phase error, (b) optimized pump pulse carrier envelope phase ϕ_p shown as a function of the target phase ϕ_t , (c) optimized pulse envelope, showing a clear distinction between pump (earlier) and Stokes (later) component.

Our optimal control calculations suggest a sequential mechanism whereby first the intermediate state is populated and then the second pulse component acts to transfer population and phase information to the desired state. Exploiting this intuition, the pulse sequences can be engineered further by optimizing each step individually, in order to (i) explore large areas of pulse parameter space for maximum performance or (ii) obtain simple pulses with near-optimal performance that are also consistent with experimental constraints. Optimizing a Gaussian-shaped Stokes pulse starting from the intermediate state, we find complete population transfer to the valence state for a pulse duration of 0.5 fs and a peak intensity of 2.4×10^{15} W/cm², corresponding to a pulse energy of $0.71 \mu\text{J}$ for a $10 \mu\text{m}$ diameter of the spot size. Longer Stokes pulses perform similarly well. Complete population transfer is achieved by 5 fs and 30 fs pulses with peak intensities of 3.4×10^{13} and 3.3×10^9 W/cm², corresponding to powers of $0.10 \mu\text{J}$ and $0.02 \mu\text{J}$, respectively. Populating the intermediate state efficiently by the pump pulse is thus identified to be the limiting step.

The performance of the pump step is analyzed in Fig. 4 for Gaussian pulses with different pulse durations (a) and energies (b): At a given energy, the maximum intermediate state population first increases with pulse duration ($\sigma \leq 50$ fs). This is explained by a better selectivity of longer, i.e., spectrally narrower pulses, which avoid populating other resonances nearby. However, for very long pulses, the maximum intermediate state population decreases due to the lifetime of the intermediate state, which is about 25 fs [33]. Increasing the pulse energy for a given duration moves the intermediate state population maximum to earlier times and achieves larger maxima for a duration of 100 fs. However, for the smaller powers considered, increasing pulse duration can lead to a decrease in the population maximum (Fig. 4(c)). The best compromise in terms of pulse power and performance is found for a 50.0 fs/71 μJ pulse (with peak intensity of

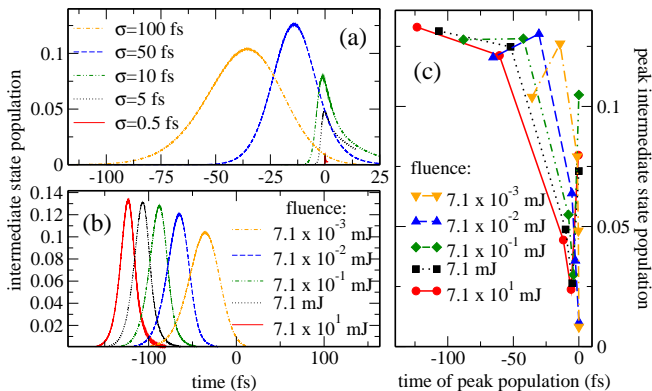


FIG. 4. (Color online) Exploring the performance of Gaussian pump pulses: Intermediate state population as a function of time ($t_{0,p} = 0$) for (a) different pulse durations at a pulse energy of $7.1 \mu\text{J}$, and (b) different pulse energies for a FWHM of 100.0 fs . As pulse duration increases, larger intermediate state populations can be achieved, although for a given energy the finite lifetime acts to drive the intermediate state population down. (c) Peak intermediate state population as a function of the time it is achieved for different pulse energies (propagations with TDCIS-HFS-1P).

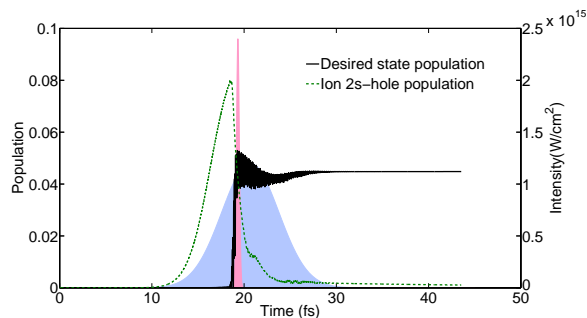


FIG. 5. (Color online) 2s hole population (dashed green line), corresponding mainly to the intermediate state, and target state populations (solid black line) for a $10 \text{ fs}/7.1 \mu\text{J}$ pump pulse and a $0.5 \text{ fs}/0.71 \mu\text{J}$ Stokes pulse centered at 18.7 fs (peak intensities of 1.2 and $2.4 \times 10^{15} \text{ W/cm}^2$, respectively). Pulse sequences are shown in light blue (pump) and red (Stokes).

$2.4 \times 10^{15} \text{ W/cm}^2$) which achieves a maximum intermediate state population of 0.130 , only slightly smaller than the peak at 0.133 seen in Fig. 4(b) for $100.0 \text{ fs}/71 \text{ mJ}$ ($1.2 \times 10^{18} \text{ W/cm}^2$) pulse.

Improved pulse sequences may now be obtained by setting the Stokes pulse maximum to coincide with the maximum intermediate state population, using the pulse energy that balances the incidental transfer to undesired states with the intermediate state lifetime. An example is shown in Fig. 5, yielding a Raman state population of 4.5% , compared to the 7.9% maximum intermediate state population. We find final target populations of 13% , using TDCIS-HFS-1P, when increasing the pump duration to 50 fs , keeping pump energy and Stokes duration and

energy fixed. Such pump pulse parameters are feasible at free electron laser (FEL) facilities where it might prove difficult to realize sub-femtosecond Stokes pulses, however, but longer Stokes pulses may be employed as discussed above. When using these sequences of Gaussian pulses as initial guess for further optimization with Krotov's method, only small improvements are found. This suggests these sequences to be already close to optimal.

The simplicity of our pump-Stokes sequences raises the question whether other commonly used schemes perform equally well. This is not the case: For example, merely increasing the amplitudes for a set of simultaneous pulses achieves target populations of 0.2% at most, for a pulse intensity of 10^{16} W/cm^2 , before competing population transfers to other states and ionization take over and the populations fall again. This approach also does not provide the phase control needed to reach arbitrary superposition states. Another candidate is stimulated Raman adiabatic passage (STIRAP) [34] where the Stokes pulse precedes the pump to avoid population of the intermediate state and thus the detrimental effect of the intermediate state lifetime. However, given the couplings and energies of coherent xuv Raman excitation in neon, adiabatic transfer is found to be possible only when unrealistically long pulses of hundreds of picoseconds to nanoseconds are employed.

This work presented a combined coherent quantum control and electronic structure method which optimizes the population and coherence of an xuv Raman excitation of an atom. The method is unique in that it includes the effects of both channel coupling and ionization, together with a powerful technique of optimal coherent control. The optimal control approach yields locally optimal forms of the laser pulses and also reveals insight into the physical mechanism of the continuum-mediated coherent Raman excitation. This allows a relatively simple pathway model to be employed for generation of sequential pulse schemes that can be tailored to specific experimental constraints without loss of fidelity.

For the Ne example studied here, we found a sequential intermediate state-Raman state excitation to be optimal and identified the limiting step to be populating the intermediate resonance from the ground state. In contrast, a counterintuitive STIRAP pulse sequence was found to be unfeasible, due to the small coupling between the ground and intermediate state. A 50 fs , $7.1 \mu\text{J}$ pump pulse populates the intermediate state up to 13% , and this population can be completely transferred to the Raman state with various Stokes pulses, for example with a duration of 0.5 fs and an energy of $0.71 \mu\text{J}$, or 30 fs and $0.02 \mu\text{J}$. Most important for the realization of coherent multi-dimensional spectroscopies, we showed that it is possible to excite a superposition of the Raman and ground states with a controllable relative phase. Here the primary control knob was found to be the carrier envelope phase of the pump pulse. The pulse intensities

and durations we have determined here are in principle possible to realize with FELs, in particular seeded FELs such as FERMI@Elettra that provide the required time resolution to compete with the resonance lifetime. The optimized coherent Raman calculations thus provide design principles for future FELs, especially in regard to the need for multiple beamlines in order to implement a multidimensional x-ray spectroscopy scheme and the choice of frequencies.

The sequential pump-Stokes scheme illustrated here can readily be applied to other atoms. Indeed, order-of-magnitude estimates of required pulse durations and intensities can be obtained for atoms with isolated resonances, analogous to the neon 2s-3p resonance utilized here, by comparing the transition dipole strengths of the desired levels with the neon levels. More detailed calculations will be required for overlapping resonances, where longer pulses may be required to preferentially address one resonance over the other, or alternate mechanisms for Raman excitation may arise which utilize both (or many) resonances. Such pulses should also work well in molecules, since the intermediate state is localized (atom-like) and driving the population into this state is the limiting step. With this demonstration of the key elements of state-selective population transfer and excitation of superposition states, coherent multidimensional spectroscopies capable of probing the dynamics of valence excitations in molecules via localized core-hole excitations, such as pump-probe and coherent x-ray Raman scattering (CXRS) [8], now appear feasible. The present work illustrates the usefulness and promise of the coherent control approach in bringing techniques such as CXRS to fruition under the challenging environment of atomic and molecular ionization continua.

The authors would like to thank Michael Goerz and Daniel Reich for assistance with the Krotov control code, and Stefan Pabst and Robin Santra for help with the XCID TDCIS code. Additionally, we would like to acknowledge Xuan Li, Bill McCurdy, Dan Haxton, Ali Belkacem and Holger Mueller for helpful discussions. We acknowledge computational resources obtained under NSF award CHE-1048789 and travel assistance provided by NSF international collaboration grant OISE-1158954 and the DAAD.

* whaley@berkeley.edu

- [1] D. S. Larsen, K. Ohta, Q.-H. Xu, M. Cyrier, and G. R. Fleming, *J. Chem. Phys.* **114**, 8008 (2001).
- [2] S. Mukamel, *Annu. Rev. Phys. Chem.* **51**, 691 (2000).
- [3] D. M. Jonas, *Annu. Rev. Phys. Chem.* **54**, 425 (2003).
- [4] G. Engel, T. Calhoun, E. Read, T.-K. Ahn, T. Manl, Y.-C. Cheng, R. Blankenship, and G. Fleming, *Nature* **446**, 782 (2007).
- [5] X. Li, T. Zhang, C. N. Borca, and S. T. Cundiff, *Phys. Rev. Lett.* **96**, 057406 (2006).
- [6] M. Erementchouk, M. N. Leuenberger, and L. J. Sham, *Phys. Rev. B* **76**, 115307 (2007).
- [7] L. Yang and S. Mukamel, *Phys. Rev. B* **77**, 075335 (2008).
- [8] S. Tanaka and S. Mukamel, *Phys. Rev. Lett.* **89**, 43001 (2002).
- [9] S. Mukamel, D. Abramavicius, L. Yang, W. Zhuang, I. Schweigert, and D. Voronine, *Accounts of Chemical Research* **42**, 553 (2009).
- [10] M. Shapiro and P. Brumer, *Quantum Control of Molecular Processes* (Wiley Interscience, 2012).
- [11] D. D'Alessandro, *Introduction to Quantum Control and Dynamics* (Chapman & Hall/CRC, 2007).
- [12] V. Zeman, M. Shapiro, and P. Brumer, *Phys. Rev. Lett.* **92**, 133204 (2004).
- [13] T. Klamroth, *J. Chem. Phys.* **124**, 144310 (2006).
- [14] M. Mundt and D. J. Tannor, *New J. Phys.* **11**, 105038 (2009).
- [15] A. Castro, J. Werschnik, and E. K. U. Gross, *Phys. Rev. Lett.* **109**, 153603 (2012).
- [16] X. Li, C. W. McCurdy, and D. J. Haxton, *Phys. Rev. A* **89**, 031404 (2014).
- [17] T. K. Allison, T. W. Wright, A. M. Stooke, C. Khurmi, J. van Tilborg, Y. Liu, R. W. Falcone, and A. Belkacem, *Opt. Lett.* **35**, 3664 (2010).
- [18] L. Greenman, P. Ho, S. Pabst, E. Kamarchik, D. Mazziotti, and R. Santra, *Phys. Rev. A* **82**, 023406 (2010).
- [19] S. Pabst, L. Greenman, , and R. Santra, XCID program package for multichannel ionization dynamics, Rev. 629, with contributions from P. J. Ho. DESY, Hamburg, Germany, 2011.
- [20] S. Pabst, L. Greenman, D. A. Mazziotti, and R. Santra, *Phys. Rev. A* **85**, 023411 (2012).
- [21] S. Pabst, L. Greenman, P. Ho, D. Mazziotti, and R. Santra, *Phys. Rev. Lett.* **106**, 53003 (2011).
- [22] A. Wirth, M. T. Hassan, I. Grguraš, J. Gagnon, A. Moulet, T. Luu, S. Pabst, R. Santra, Z. Alahmed, A. Azzeer, et al., *Science* **334**, 195 (2011).
- [23] S. Pabst, A. Sytcheva, A. Moulet, A. Wirth, E. Goulielmakis, and R. Santra, *Phys. Rev. A* **86**, 063411 (2012).
- [24] A. Sytcheva, S. Pabst, S.-K. Son, and R. Santra, *Phys. Rev. A* **85**, 023414 (2012).
- [25] A. Goldberg and B. W. Shore, *J. Phys. B* **11**, 3339 (1978).
- [26] R. Santra and L. S. Cederbaum, *Phys. Rep.* **368**, 1 (2002).
- [27] A. I. Konnov and V. A. Krotov, *Automation and Remote Control* **60**, 1427 (1999).
- [28] A. Bartana, R. Kosloff, and D. J. Tannor, *Chem. Phys.* **267**, 195 (2001).
- [29] J. P. Palao, R. Kosloff, and C. P. Koch, *Phys. Rev. A* **77**, 063412 (2008).
- [30] D. Reich, M. Ndong, and C. Koch, *J. Chem. Phys.* **136**, 104103 (2012).
- [31] The presence of matrix transposes instead of the usual Hermitian conjugates is due to the use of a CAP.
- [32] J. Duoandikoetxea and D. Cruz-Urbe, *Fourier analysis* (American Mathematical Society, 2001).
- [33] K. Codling, R. P. Madden, and D. L. Ederer, *Phys. Rev.* **155**, 26 (1967).
- [34] K. Bergmann, H. Theuer, and B. W. Shore, *Rev. Mod. Phys.* **70**, 1003 (1998).